# Surface reactions of gold(111) with aqueous cyanide studied by scanning tunneling microscopy

Robin L. McCarley, and Allen J. Bard

## More About This Article

The permalink http://dx.doi.org/10.1021/j100197a051 provides access to:

- Links to articles and content related to this article
- Copyright permission to reproduce figures and/or text from this article

(20) Demontis, P.; Suffritti, G. B.; Quartieri, S.; Fois, E. S.; Gamba, A. *J. Phys. Chem.* **1988,** *92,* 867.

(21) Demontis, P.; Fois, E. S.; Suffritti, G. B.; Quartieri, S. *J. Phys. Chem.* **1990,** *94,* 4329.

(22) Fitch, A. N.; Jobic, H.; Renouprez, A. *J. Phys. Chem.* **1986,** *90,* 1311.

(23) Kiselev, A. V.; Du, P. Q. *J. Chem. Soc., Faraday Trans. 2* **1981,** *77,* 1.

(24) Bezus, A. G.; Kiselev, A. V.; Lopatkin, A. A.; Du, P. Q. *J. Chem. Soc., Faraday Trans. 2* **1978,** *74,* 367.

(25) Ewald, P. P. *Ann. Phys.* **1921,** *64,* 253.

(26) Ángyán, J. G.; Colonna-Cesari, F.; Tapia, O. *Chem. Phys. Lett.* **1990,** *166,* 180.

(27) Verlet, L. *Phys. Rev.* **1967,** *159,* 98.

(28) Berendsen, H. J. C.; Postma, J. P. M.; van Gunsteren, W. F.; DiNola, A.; Haak, J. R. *J. Chem. Phys.* **1984,** *81,* 3684.

(29) Willis, B. T. M.; Pryor, A. W. *Thermal Vibrations in Crystallography*; Cambridge University Press: Cambridge, 1975.

(30) Black, J. E.; Bopp, P. *Surf. Sci.* **1987,** *182,* 98.

(31) Johnson, C. K. ORTEP: *A* FORTRAN *Thermal Ellipsoid Plot Program*; ORNL-3794, Oak Ridge National Laboratory, Oak Ridge, TN, 1965.

(32) Richardson, J. W.; Pluth, J. J.; Smith, J. V.; Dytrych, W. J.; Bibby, D. M. *J. Phys. Chem.* **1988,** *92,* 243.

(33) Pluth, J. J.; Smith, J. V. *J. Am. Chem. Soc.* **1980,** *102,* 4704.

(34) Behrens, P. H.; Wilson, K. R. *J. Chem. Phys.* **1981,** *74,* 4872.

(35) de Man, A. J. M.; van Best, B. W. H.; Leslie, M.; van Santen, R. A. *J. Phys. Chem.* **1990,** *94,* 2524.

(36) Geidel, E.; Böhlig, H.; Birner, P. *Z. Phys. Chem.* **1991,** *171,* 121.

(37) Godber, J.; Ozin, G. A. *J. Phys. Chem.* **1988,** *92,* 2841.

(38) Allen, M. P.; Tildesley, D. J. *Computer Simulation of Liquids*; Claredon Press: Oxford, U.K., 1987.

# Surface Reactions of Au(111) with Aqueous Cyanide Studied by Scanning Tunneling Microscopy

**Robin L. McCarley and Allen J. Bard\***

*Department of Chemistry and Biochemistry, The University of Texas at Austin, Austin, Texas 78712*
*(Received: February 4, 1992; In Final Form: May 18, 1992)*

Dilute solutions ($10^{-4}$–$10^{-5}$ M) of aqueous cyanide cause the formation of monolayer pits on Au(111) as studied by scanning tunneling microscopy (STM). The roughly triangular etch pits on the (111) terraces reflect the 3-fold rotational symmetry of the fcc Au(111) crystal and appear to form at atomic defects on the terrace. In situ STM of the pitted Au(111) surface in $5 \times 10^{-5}$ M KCN shows that the pits collapse in minutes due to enhanced mobility of Au atoms from adsorbed cyanide. A mobile step edge/adatom diffusion model is used to explain the nature of the pit collapse. This is the first STM study of in situ *monolayer* pit formation and annealing in an aqueous chemical etchant.

## Introduction

We report here in air and in situ atomic scale STM images of Au(111) films on mica undergoing dissolution and annealing in dilute, aqueous cyanide solutions. At high concentrations of cyanide ($>10^{-4}$ M) in the presence of oxygen, complete disruption of the Au(111) surface takes place in less than 1 min, but lower cyanide concentrations ($10^{-4}$ M $<$ [CN$^-$] $< 10^{-5}$ M) result in slow dissolution of the Au(111) with the formation of monolayer deep, triangular etch pits reflecting the geometry of the fcc surface. These pits heal as a result of mobile surface atoms which fill in the pits at rates independent of pit size.

Identification of reactive sites on surfaces with chemical etchants has led to a better understanding of the role surface defects play in interfacial chemistry.[1] Corrosion,[2] adsorption,[3] catalysis,[4] and surface reconstruction[5] are just some of the processes which are influenced by defect structures. In particular, the effects of dislocations on metal dissolution reactions are important in the study of dealloying and corrosion, where loss of complexed metal is primary in the surface reaction sequence.[2] Most methods used to investigate dissolution processes are based on optical or electron microscopic analysis of a surface which has been chemically etched so as to accentuate the dislocations on the surface. Such dislocation etching of well-defined (single crystalline) materials usually results in the formation of multilayer, micron-sized pits which reflect the geometry of the given crystal face.[1] However, because these pits must be rather large for microscopic imaging, two or more atomic defects may have coalesced to form a single etch pit, causing loss of information on an atomic scale. Moreover, ex situ etch pit techniques do not allow real time studies of dissolution dynamics and surface diffusion while the specimen is in the chemical environment.

The fundamental stages in the chemical etching of most surfaces are etchant adsorption, complexation (or oxidation) of the surface species, and dissolution. Precipitation of products onto the surface can also play a major role because such an event can alter the dissolution rate and even stop dissolution.[1] In the chemical etching of metals, especially alloys, surface self-diffusion is important in the reestablishment of a stable surface and in the exposure of underlying defect sites, which also react and dissolve.[2] Surface self-diffusion is then expected to affect the shape and size distribution of etch pits. Once pits are formed, mobile atoms may increase or decrease pit size depending on the location or size of the pit or quantity of adsorbed species (etchant or impurities) on the surface. In an atomic force microscopic study of calcite dissolution, impurity adsorbates were shown to affect the distribution of etch pit size and shape.[6] This has also been demonstrated in our laboratories during the formation of etch pits on highly oriented graphite (HOPG).[7] Thus, a better understanding of the role adsorption and surface self-diffusion play in the dissolution process of metals would lend insight to the mechanism of etch pit formation.

Scanning tunneling microscopy (STM)[8] can be used to observe processes with atomic resolution in liquid environments, if faradaic processes are minimized at the tip.[9] Examples include imaging of electrode surfaces under potential control[10] and examination of biological materials under solution.[11] A recent in situ electrochemical STM study demonstrated that atomic level imaging of potential-induced surface reconstructions on Au(100) is possible and indicated that the reconstruction occurs at a rate much slower than that evidenced solely from the electrochemical data.[5] Thus, the kinetics of surface reactions on an atomic or molecular scale, as well as the location of site specific surface reactions, which may be quite different than that assumed from other techniques, can be probed by in situ STM.

## Experimental Section

**Chemicals.** High-purity water (Millipore Milli-Q purification system, $>$18 M$\Omega$ cm) was used throughout. Anhydrous methanol (Photrex, J. T. Baker) was used without further purification. Potassium cyanide (A.C.S. Grade, Fisher) and KAu(CN)$_2$ (98%, Aldrich) were used as received. All other chemicals were reagent grade or better.

**Instrumentation.** Images were obtained with a NanoScope II scanning tunneling microscope (Digital Instruments, Santa Barbara, CA) using mechanically cut (GC Electronics diagonal cutters, "dikes") Pt/Ir (80:20) tips. Large-scale scans were obtained in the topographic mode (constant current) and atomic resolution images acquired in the constant-height mode. If necessary, images were slightly filtered using the low pass filter option of the NanoScope II software. Tips for in situ work were insulated with clear fingernail polish (Wet 'n Wild, Pavion Ltd.). For in situ experiments an 8-$\mu$L drop of the KCN solution was placed on the Au substrate, and the tip was lowered into this drop. A small container of water was placed inside the microscope assembly to minimize solvent evaporation during the course of the experiment.

Infrared measurements were made on a Nicolet 60SXR FTIR spectrometer fitted with a liquid nitrogen cooled MCT detector and a Harrick Model RMA-00G reflection attachment. Grazing incidence spectra were collected at 84° with 4-cm$^{-1}$ resolution on 150-nm Au films on Si(111) wafers.

**Substrates.** Au(111) films (150–250 nm) were prepared by thermal evaporation[12] of high-purity Au (99.99%) at 0.2 nm s$^{-1}$ onto heated mica in a Plasmatron P-30 thin film system operating at $2 \times 10^{-6}$ Torr vacuum. The mica (Asheville-Schoonmaker, Newport News, VA) was heated to 310 °C and held there for 30 min before deposition was carried out. Once the substrates had cooled to near 100 °C, the chamber was back-filled with nitrogen and the Au/mica films were stored in the laboratory ambient. Polycrystalline Au films on Si(111) wafers were made by evaporation of 150 nm of Au onto 5 nm of Cr that had been deposited on freshly cleaned Si(111). The Si(111) was cleaned by dipping in 1:3 H$_2$O$_2$ (30%):H$_2$SO$_4$ for 5 min (*these solutions must be handled with caution due to their strong oxidizing power*), followed by rinsing in deionized water for 5 min and then blowing dry in Ar.

## Results and Discussion

**Dissolution of Au(111): Ex Situ Imaging.** A constant-current STM image of bare Au(111) on mica in air is shown in Figure 1A; monatomic step terraces of up to 300 nm in width are found routinely on these epitaxially prepared films. An atomic resolution, constant-height image of the Au(111) surface in air is displayed in Figure 1B. The distance between the nearest-neighbor atoms is 0.29 ± 0.02 nm, consistent with previous reports for Au(111) surfaces.[13–15] Upon immersion in 10$^{-2}$ M KCN in the laboratory ambient for 1 min, rinsing with water, and blowing dry in Ar, the surface is seen to be severely damaged (Figure 2A). The large, flat plateaus are no longer present, and deep crevices dominate the surface. We do not see this behavior after immersion in CN$^-$-free solutions or solutions with anions like Cl$^-$. Longer exposure times in 10$^{-2}$ M KCN (8 h) caused the film to completely dissolve from the mica; this corresponds to a rate of dissolution of approximately one monolayer per minute. The rate of Au dissolution by CN$^-$ in the presence of O$_2$ is greatly decreased at lower CN$^-$ concentrations as demonstrated in Figure 2B,C, where the Au was exposed for 2 min to 10$^{-3}$ and $5 \times 10^{-5}$ M solutions of CN$^-$, respectively. At 10$^{-3}$ M there are still some atomically flat terraces, but the size of the smooth areas is reduced to approximately 30 nm. Examination of Figure 2B indicates that the dissolution has caused the crystallites to etch at the edges (noticeably more so near the top), producing a tapered or cone-shaped structure. Further evidence for dissolution at the crystallite step edges is shown in Figure 2C with [CN$^-$] = $5 \times 10^{-5}$ M. The edges of the grain are noticeably "serrated"; i.e., they have a series of connected triangular shapes, and the grain boundaries are much more pronounced due to loss of material. Note the small, topmost layer of Au in the upper right of Figure 2C; the surface appears to have dissolved layer by layer from the edges or defect sites. We do not see any pits forming inside another pit, i.e., double pits.

Most noticeable in Figure 2C are the roughly triangular pits in the (111) terrace. When low concentrations of CN$^-$ were used, pits of this shape and size were reproducibly found on the crystallites, but the number and size varied depending on [CN$^-$] and
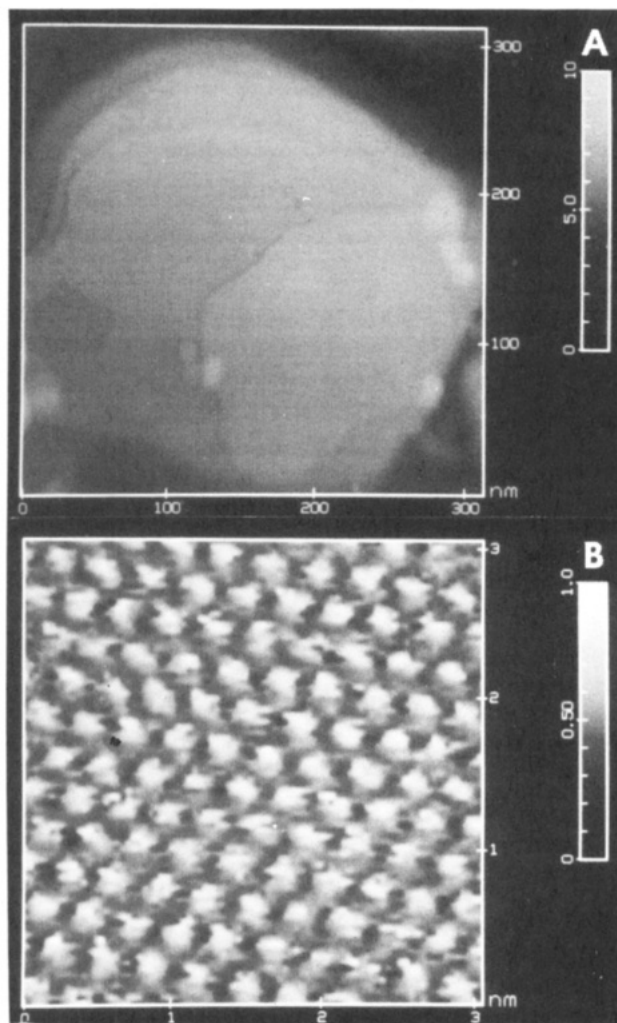


**Figure 1.** (A) A 310- × 310-nm constant-current image of bare Au-(111)/mica. Gray scale is 0–20 nm; $i_t$ = 2 nA; $V_t$ = 50 mV. (B) An unfiltered 3- × 3-nm constant-height image of bare Au(111); $i_t$ = 3 nA; $V_t$ = 20 mV.

time. The cross-sectional view in Figure 2E demonstrates that the pits are indeed monatomic, with the measured depth of 0.24 nm being in good agreement with previous reports for Au(111).[12] In this experiment the pits were not very mobile while scanning or merely storing in the laboratory ambient; a pitted Au sample imaged after residing a week on the benchtop still displayed the monatomic pits. A typical distribution of pit sizes is indicated in Figure 2D, which shows an area of a terrace that has many different-sized pits as well as pits which have coalesced to form one large pit or an isolated terrace ledge. From Figure 2C it appears that pit shape and orientation are the same over all the surface. Such triangular pits (angles are approximately 60°) are characteristic of a (111) fcc crystal;[1] micron-sized triangular pits have been observed by optical microscopy for Au(111) single crystals exposed to dislocation etching solutions such as aqua regia.[16] The fact that the pits have the same orientation is also indicative of dissolution along crystallographic directions, although we have yet to assign lattice vectors from our atomic resolution images of the surface. We feel the approximate triangular nature of the pits is a result of surface self-diffusion of Au atoms (see discussion below) and possibly different etching rates near and far from the etch pit vertices. The formation of pits on Au is quite different from those on HOPG,[7] since the carbon atoms are bonded to each other on HOPG and cannot move on the surface, whereas Au atoms are quite mobile in aqueous CN$^-$ media. Rapid diffusion of Au atoms during the dissolution process, coupled with variations in the surface defect density, may explain the pit size distribution. Variations in the size distribution of pits (on a nanometer scale) on calcite during dissolution have been noted by Hillner et al.[6]
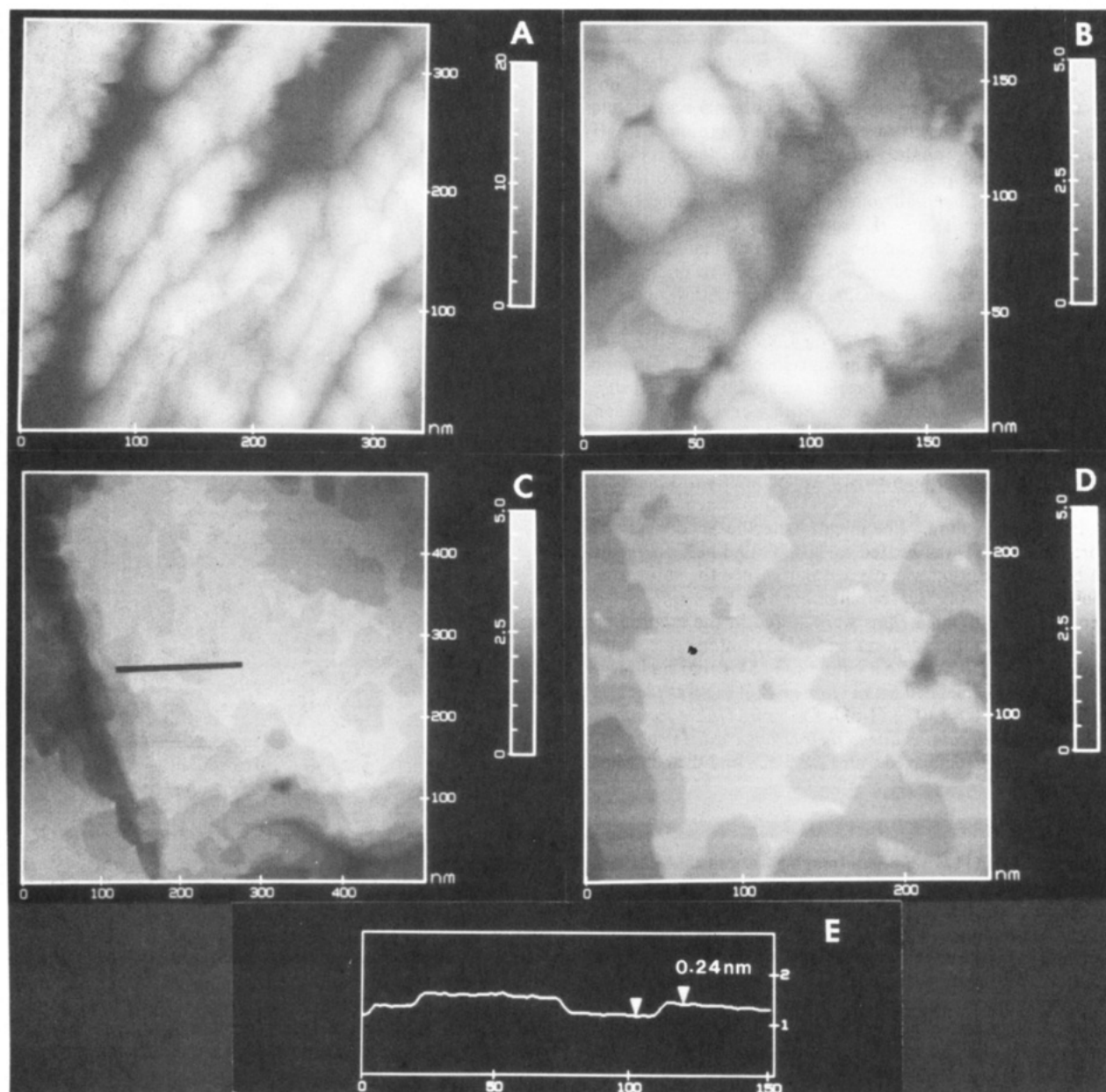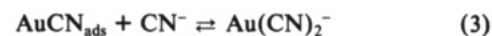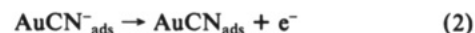
**Figure 2.** Constant-current images of Au(111). (A) A 350- × 350-nm area treated with $10^{-2}$ M KCN for 1 min. Gray scale is 0–20 nm. (B) A 175- × 175-nm region treated with $10^{-3}$ M KCN for 1 min. Gray scale is 0–5 nm. (C) A 500- × 500-nm area treated with 5 × $10^{-5}$ M KCN for 2 min. Gray scale is 0–5 nm. (D) Same as (C) but different 250- × 250-nm area. (E) Line-scan shown in (C) displaying monatomic nature of pits. Tunneling parameters for all images are $i_t$ = 1 nA and $V_t$ = 50 mV.

In the present study the etch pits continuously grow with exposure time and do not seem to form, diffuse, and coalesce by a vacancy clustering mechanism.[17] There is some correlation of pit size with exposure time, but it is difficult to quantitatively assess this effect from our data. Most unique to this study is the observation of *monolayer* etch pits; there is only one other study using scanning probe microscopy to investigate growth of monolayer pits in a chemical etchant solution,[6] and that study was concerned with calcite, an insulator.

It is well understood why dissolution takes place at edges or defects on a crystal surface, while formation of pits on a perfect (111) plane is less energetically favorable. We therefore believe that the pits form on the terraces at atomic defects which act as nucleation sites for pit growth. These defects could be single atom vacancies or impurities in the (111) plane or possibly screw dislocations. Ideally, one would like to image such atomic defects before introduction of the chemical etchant and follow the growth of those defects during the etching process. Alternatively, the rate of dissolution at the step edges could be slower than the flux of etchant to the surface, and therefore dissolution would be possible on the (111) plane. We do not feel this to be the case here, for

even at low concentrations of cyanide, $10^{-5}$ M, pits form on the terraces in approximately equal number to those at higher [$CN^-$].

The steps involved in the Au dissolution process in the presence of $O_2$ and $CN^-$ have been proposed as follows[18]

$$Au + CN^- \rightleftharpoons AuCN^-_{ads} \qquad (1)$$

$$AuCN^-_{ads} \rightarrow AuCN_{ads} + e^- \qquad (2)$$

$$AuCN_{ads} + CN^- \rightleftharpoons Au(CN)_2^- \qquad (3)$$

where $O_2$ is the oxidant in eq 2 in either a two- or four-electron process to give overall

$$4Au + 8CN^- + O_2 + 2H_2O \rightarrow 4Au(CN)_2^- + 4OH^- \quad (4)$$
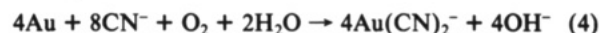
For the present study we will assume a four-electron process to yield hydroxide. Thus, from eqs 1 and 2 we see that adsorption of $CN^-$ and the presence of a sufficiently potent oxidant are needed for the dissolution of Au. Electrochemical experiments have shown that the potential for oxidation of Au is shifted negatively by nearly 2 V by adsorption of $CN^-$, thus allowing $O_2$ to serve as the oxidizing agent.[18] We have confirmed the presence of adsorbed CN
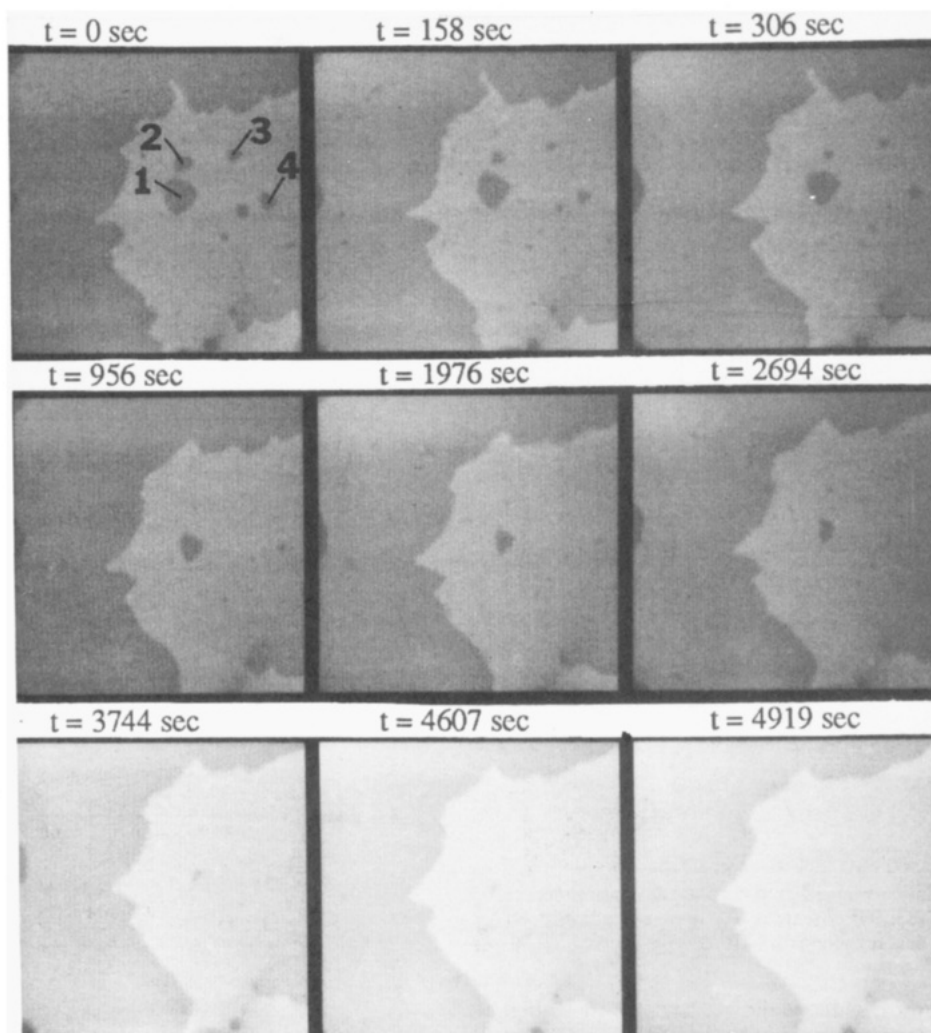
**Figure 3.** In situ constant-current images at different times for a 200- $\times$ 200-nm section with [CN$^-$] = 5 $\times$ 10$^{-5}$ M. Gray scale is 0–5 nm.

on the Au surfaces with grazing incidence infrared spectroscopy. Only one infrared-active mode associated with adsorbed CN at 2127 cm$^{-1}$ was found on Au films treated with 10$^{-4}$ M KCN solutions in the presence of O$_2$, in agreement with previous reports.[19] This peak has been attributed to linearly adsorbed CN, as demonstrated by polarized infrared spectroelectrochemistry.[19]

To determine the effect of O$_2$ on the observed behavior, experiments were carried out in an inert atmosphere box with low levels of O$_2$ present (<10 ppm) in methanol. Such samples displayed extremely slow dissolution rates, indicating that O$_2$ is necessary to form the pits observed in this study. (The solubility of O$_2$ in H$_2$O and MeOH is 1 part in 32 and 1 part in 7 by volume at 20 °C, respectively.) No attempts were made to use another oxidant. In addition, 10$^{-4}$ M aqueous solutions of Au(CN)$_2^-$ did not cause pitting of bare Au nor increases in pit size for CN$^-$-treated Au, confirming the stability of the Au(CN)$_2^-$ complex ($K_{diss}$ = 2.5 $\times$ 10$^{-29}$) and the need for free CN$^-$ for dissolution. In addition, the stability of Au(CN)$_2^-$ is indicated by its very negative reduction potential. Thus, we feel that our results are consistent with the proposed mechanism above for the cyanidation of Au in the presence of O$_2$.

**In Situ STM of Au(111) in CN$^-$.** Imaging Au(111) under a 5 $\times$ 10$^{-5}$ M KCN$_{(aq)}$ solution is demonstrated in Figure 3. At $t$ = 0 the surface is already pitted, although the time to place the solution on the Au(111) and reassemble the microscope was fairly short, approximately 60 s. Attempts to slow the kinetics by lowering the [CN$^-$] so as to observe the pits form were unsuccessful; even at 10$^{-5}$ M KCN very small pits had already formed and did not increase in size as a function of time. Lowering the temperature of the microscope was not carried out. If one observes the same area over time with the STM, the pit sizes do not increase

with time but rather decrease (Figure 3). We speculate that the pits stop growing due to depletion of the [CN$^-$] (not O$_2$) in the solution, because if more CN$^-$ solution is added, the surface begins to dissolve again. (If all the cyanide were to react stoichiometrically with the Au, about 3–5 monolayers of Au would dissolve for the 8-$\mu$L drop of [CN$^-$] = 5 $\times$ 10$^{-5}$ M.) Wadsworth[20] and Kudryk[21] have shown that the kinetics of Au dissolution in CN$^-$/O$_2$ are controlled by CN$^-$ diffusion at CN$^-$ concentrations up to about 10$^{-3}$ M and by O$_2$ diffusion above this concentration of CN$^-$. The kinetic model[20] that explained the experimental observations of Kudryk[21] is based on mixed diffusion of CN$^-$ and O$_2$ to the Au surface, followed by charge transfer. Such a model predicts a depletion layer for CN$^-$ near the Au surface (a concentration gradient), which grows out into solution with time. Thus, the rate of dissolution drops to low values after the concentration gradient has become small. Within the concentration range studied (10$^{-5}$–10$^{-4}$ M) the kinetic model predicts the initial pit size (i.e., at approximately 1 min after immersion) should be proportional to CN$^-$ concentration. A plot of initial pit size versus CN$^-$ concentration is displayed in Figure 4, demonstrating that pit size varies directly with CN$^-$ concentrations up to 10$^{-4}$ M, where the rate starts to depend on O$_2$ diffusion. These results are in good agreement with the model proposed by Wadsworth.[20] As the pits collapse, the step edges tend to smoothen or straighten out with time. Although there is probably some tip/substrate interaction, we feel, on the basis of control experiments, that this does not cause the filling of pits. The pits fill in *all* over the surface in this in situ experiment, not just in the scanned area. A larger area scanned after that in Figure 3 is displayed in Figure 5, with the region scanned in Figure 3 denoted by the box. Pits present in Figure 5 before scanning the area in Figure 3 are now also
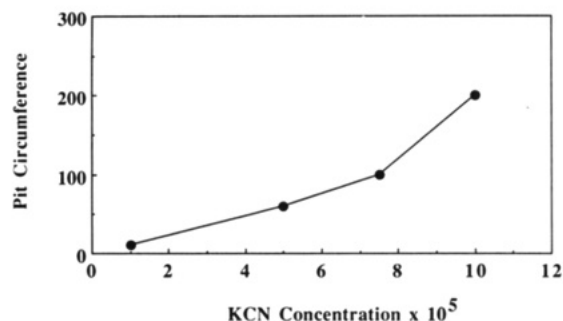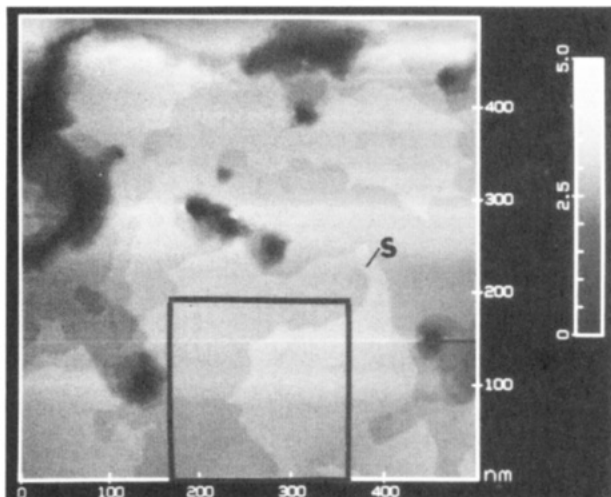
**Figure 4.** Pit circumference versus [CN⁻].



**Figure 5.** In situ constant-current image for a 500- × 500-nm section with [CN⁻] = 5 × 10⁻⁵ M. Gray scale is 0–5 nm. Box shows area scanned in Figure 3. S denotes screw dislocation. $i_t$ = 1 nA; $V_t$ = 50 mV.



**Figure 6.** Schematic of (A) vacancy annihilation model and (B) adatom diffusion model.



**Figure 7.** Pit circumference normalized to initial circumference. (A) [CN⁻] = 5 × 10⁻⁵ M; (B) [CN⁻] = 7.5 ~ 10⁻⁵ M.

annealed. Since the unscanned area did not have the tip acting on it during the time (approximately 5000 s) of that in Figure 3 and the pits still healed, we feel the annealing process does not depend on tip/substrate interactions. This has been confirmed by imaging in situ, retracting the tip, and then reimaging to reveal the annealed surface.

Before we discuss the kinetics of pit healing, a closer look at Figure 5 is in order. To the right of the dashed box in Figure 5 is a screw dislocation labeled S. There does not appear to be a high rate of etching at this defect in comparison to the other areas of the surface. This result is quite surprising, since screw and slip dislocations have been shown to dissolve preferentially. With our in situ STM experiments we have noted many screw dislocations which did not appear to etch. We do not have an explanation for this observation but feel that it points to a different dissolution and annealing mechanism, as discussed below.

It is energetically favorable to reduce the number of edge atoms by diffusion of atoms to the pit, i.e., to reestablish the (111) plane. We do not see pit motion toward a step edge, but rather the pits collapse or fill in as the terrace edge loses material. Measuring the difference in material at terrace edges for Figure 3 at $t$ = 0 s and $t$ = 4919 s and comparing this to the original pit areas at $t$ = 0 s gives 86 300 and 84 600 Å², respectively. Thus, there is ample material lost from the step edge to fill the pits. In situ electrochemical STM studies of oxidized Au(111) in ClO₄⁻ media[22] point to "vacancy clustering" (pits merging to form bigger pits) followed by "vacancy annihilation" (pit movement to edges) to "expel" pits from the (111) surface (Figure 6A). We do not find this with our Au/CN⁻ system and feel that the annealing mechanism in this case is different. The pits in the present study appear to anneal by diffusion of adatoms from terrace edge sites to the pits (Figure 6B). There is no indication of localized surface atoms (adatoms) in any of the STM scans, even though there should be many of these at the given annealing rate of the pits. This may be explained by comparing the speed at which these
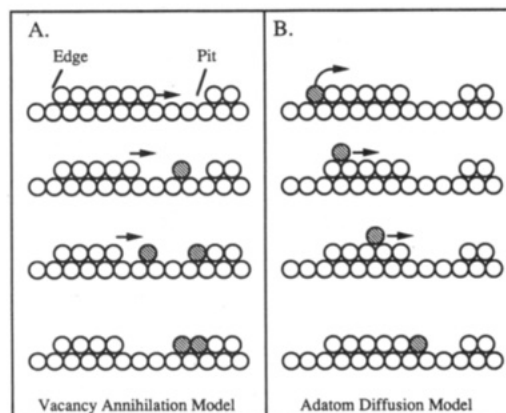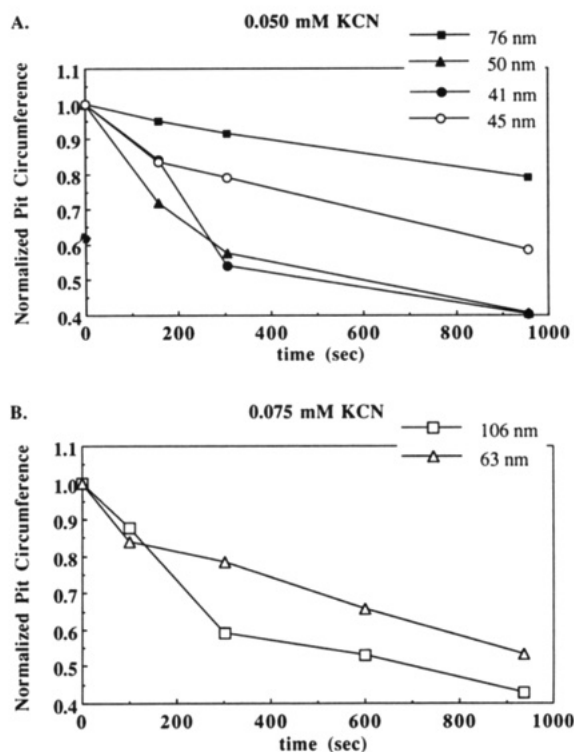
events occur and the time necessary to acquire the STM images. The response time of the acquisition electronics is probably too slow to observe a diffusing atom. Moreover, an isolated adatom would probably be pushed by the scanning tip, given the strong tip/substrate forces and the weak binding of an adatom (at ambient temperature). Although we have no direct STM evidence of adatoms on the surface, we feel that diffusion of adatoms to the pits is the most likely explanation, since a vacancy annihilation mechanism does not fit with our results. Neither does a "step edge atom jumping" mechanism.[23] The results presented here support diffusion of removed step edge atoms as adatoms to the pits. In addition, removal of a step edge atom and diffusion of that atom to a vacancy is generally considered to be a very low-energy process, giving support to the mobile step edge atom/adatom diffusion model.

The kinetics of etch pit annealing (normalized pit circumference versus time) are displayed in Figure 7A,B for CN⁻ concentrations of 5 × 10⁻⁵ and 7.5 × 10⁻⁵ M, respectively. There is no preferred initial trend for pits of different size, but after some induction time, the slopes of the curves in Figure 7A,B attain a steady value of 2.8 × 10⁻⁴ s⁻¹. This rate did not depend on CN⁻ concentration (over the range studied here), but the time to reach this steady
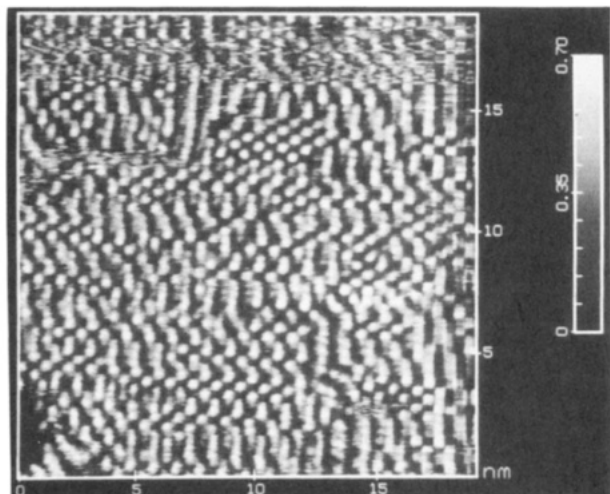
**Figure 8.** In situ atomic resolution image in $5 \times 10^{-5}$ M KCN. $i_t = 4$ nA; $V_t = 25$ mV.

rate did depend on [CN⁻]. This can be explained by Wadsworth's model,[20] where the time necessary to deplete the CN⁻ near the Au surface is dependent on CN⁻ concentration. In the early stages of the experiment both dissolution and annealing of Au are occurring; this will lead to some scatter in the size of pits produced (due to bunching of defects). Scatter in the observed changes in pit circumference is also expected because both dissolution and annealing occur. The scatter in rates should decrease as the concentration of CN⁻ is decreased in the depletion layer, leading to stable values of the annealing rate at longer times. The time necessary to obtain a stable annealing rate is then expected to be a function of initial concentration, as shown in Figure 7A,B. Thus, the rates we measure at longer times should be representative of the true annealing rate. Assuming an adatom diffusion model (Figure 6B), the annealing rate for any size pit should be constant, since diffusion of adatoms to the pits is based on a random walk. We indeed observe a constant annealing rate at long times, for all pit sizes, which is supportive of the adatom diffusion model proposed here.

The rate of diffusing material on the (111) surface is reasonable in comparison to that obtained in previous vacuum or solution STM investigations. Jaklevic et al.[24] have shown very slow room temperature annealing of Au in ultrahigh vacuum (UHV), with the self-diffusion coefficient of Au being approximately $5 \times 10^{-17}$ cm² s⁻¹ (0.5 Å² s⁻¹ or movement over 1 Au diameter in about 10 s). This UHV work dealt with intentional scratching of the surface with the tip to produce pits which healed by a mobile adatom mechanism, similar to the results here. Previous in situ STM experiments[22] demonstrated that pits created by electrochemical oxidation healed by the diffusion of the pits to step edges (vacancy annihilation) with a pit diffusion coefficient of $2 \times 10^{-15}$ cm² s⁻¹ in aqueous ClO₄⁻, a weakly adsorbed anion. Theoretically, increased Au mobility in the presence of adsorbate is caused by decreased interactions among neighboring Au atoms as a result of bonding with the adsorbates.[25] Our value for the self-diffusion coefficient of Au in CN⁻ media is approximately $4 \times 10^{-15}$ cm² s⁻¹, only slightly higher than the pit diffusion value in ClO₄⁻(aq) but much higher than the vacuum value. In situ STM work in Cl⁻, a more strongly adsorbed anion than ClO₄⁻ but weaker than CN⁻, demonstrated that pits healed faster than they could be observed on the STM time scale.[26] The pits in the present study are about 5 times larger than those in the Cl⁻ investigation and also heal by a different mechanism, allowing observation of the healing process. Although CN⁻ is more strongly adsorbed than Cl⁻, the difference in the mechanism of surface annealing must also influence the rate of annealing, with the vacancy clustering/annihilation mechanism rate (with Cl⁻) being faster than that of the mobile adatom model (with CN⁻) proposed here. Thus, we feel that CN⁻ adsorption increases the self-diffusion rate of Au in comparison to the value obtained in vacuum, and the pit

annealing mechanism results in a self-diffusion rate for Au different from previous STM studies where a vacancy annihilation mechanism applied.

To obtain more information regarding the adsorbate on the surface, constant-height imaging was performed in situ at [CN⁻] = $5 \times 10^{-5}$ M. A typical example of such an image is displayed in Figure 8. Atomic resolution images are routinely obtained in CN⁻ media with $i_t = 1$–5 nA and $V_t = 10$–50 mV. Most notable in Figure 8 are the small areas of fairly well-organized atomic species and poorly resolved "streaky" regions, indicative of mobile species on the time scale of the STM data acquisition. The image in Figure 8 was acquired at scan rates of 80 and 3.9 nm s⁻¹ in the x and y directions, respectively. We attribute the streaky features in the y direction to the relatively slow data acquisition in comparison to the diffusion rate of the surface material. Attempts to increase the y direction sampling by reducing the scan area did not improve the images substantially, indicating that the rate of surface diffusion is still higher than the acquisition time or that the tip may be interacting with the surface enough to cause instabilities in the imaging. We feel that a combination of the two could explain our inability to obtain reproducible, atomic resolution images in situ.

The spacing between the atomic structures in the more well-defined regions of Figure 8 varies from 0.55 to 0.65 nm, which is much greater than the value of 0.29 nm for Au. Two possible explanations for the image in Figure 8 are that the image is that of adsorbed CN or it shows mobile Au atoms which have no preferred arrangement on the surface. Occasionally, decreasing the tip–sample distance resulted in images with spacings characteristic of Au. The lack of reproducibility for this event makes interpretation difficult. In this experiment the tip may be imaging the adsorbate or the Au. Without data from tunneling spectroscopy it is difficult to distinguish between these two possibilities. Ex situ atomic images of CN⁻-treated Au were of poor quality and still displayed the streaky behavior. Large-scale scans did not indicate pit collapse in air, but there may be sufficient mobility or tip–sample interaction to prevent stable imaging at the atomic level. There are no reports in the literature concerning electron diffraction of Au treated with CN⁻, such as LEED. At this juncture, we cannot make a reliable assignment for the atomic species in Figure 8, although adsorbed cyanide seems more reasonable.

## Conclusions

We have described here atomic level images of Au(111) surfaces undergoing reactions in a CN⁻/O₂ media. This is the first report concerning the formation and subsequent annealing of *monolayer* pits on a metal surface caused by an aqueous solution of a chemical etchant, as studied by in situ STM. The shape of the etch pits is roughly triangular and reflects the bulk geometry of the Au(111) fcc crystal. Such pits collapse as a result of mobile surface atoms which diffuse from step edges to the pits. Although there was no observation of diffusing adatoms on the Au(111) plane, we feel confident that the pits fill in by a mobile adatom mechanism as opposed to vacancy annihilation. The measured self-diffusion rate of Au in aqueous CN⁻ media was approximately $4 \times 10^{-15}$ cm² s⁻¹, ~100 times that measured in vacuum, and is attributed to weakened Au–Au interactions caused by adsorbed cyanide.

**References and Notes**

(1) Sangwal, K. In *Etching of Crystals: Theory, Experiment, and Application*; Amelinckx, S., Nihoul, J., Eds.; North-Holland: Amsterdam, 1987.
(2) Sieradski, K.; Corderman, R. R.; Shukla, D.; Neuman, R. C. *Philos. Mag. A* **1989**, *59*, 713.
(3) Hubbard, A. T. *Chem. Rev.* **1988**, *88*, 633.
(4) Dubois, L. H.; Hansma, P. K.; Somorjai, G. A. *Appl. Surf. Sci.* **1990**, *6*, 173.

(5) Gao, X.; Hamelin, A.; Weaver, M. J. *Phys. Rev. Lett.* **1991**, *67*, 618.

(6) Hillner, P. E.; Gratz, A. J.; Manne, S.; Hansma, P. K. Submitted to *Geology*.

(7) Chang, H.; Bard, A. J. *J. Am. Chem. Soc.* **1991**, *113*, 5588.

(8) Binnig, G.; Rohrer, H. *IBM J. Res. Dev.* **1986**, *30*, 355.

(9) Cataldi, T. R. I.; Blackman, I. G.; Briggs, G. A. D.; Pethica, J. D.; Hill, H. A. O. *J. Electroanal. Chem.* **1990**, *290*, 1.

(10) Yau, S.-L.; Vitus, C. M.; Schardt, B. C. *J. Am. Chem. Soc.* **1990**, *112*, 3677.

(11) Nagahara, L. G.; Thundat, T.; Oden, P. I.; Lindsay, S. M.; Rill, R. L. *Ultramicroscopy* **1990**, *33*, 107.

(12) Chidsey, C. E. D.; Loaicono, D. N.; Sleator, T.; Nakahara, S. *Surf. Sci.* **1988**, *200*, 45.

(13) Hallmark, V. M.; Chiang, S.; Rabolt, J. F.; Swalen, J. D.; Wilson, R. J. *Phys. Rev. Lett.* **1987**, *59*, 2879.

(14) Widrig, C. A.; Alves, C. A.; Porter, M. D. *J. Am. Chem. Soc.* **1991**, *113*, 2805.

(15) McCarley, R. L.; Bard, A. J. *J. Phys. Chem.* **1991**, *95*, 9618.

(16) Hashimoto, S.; Miura, S.; Kubo, T. *J. Mater. Sci.* **1976**, *11*, 1501.

(17) Oppenheim, I. C.; Trevor, D. J.; Chidsey, C. E. D.; Trevor, P. L.; Sieradski, K. *Science* **1991**, *254*, 687.

(18) Kirk, D. W.; Foulkes, F. R. *J. Electrochem. Soc.* **1980**, *127*, 1993.

(19) Kunimatsu, K.; Seki, H.; Gorgon, W. G.; Philpott, M. R. *Langmuir* **1988**, *4*, 337.

(20) Wadsworth, M. E. *Min. Eng. (Littleton, Colo.)* **1985**, *37*, 557.

(21) Kudryk, K. V.; Kellogg, H. H. *J. Met.* **1954**, *6*, 541.

(22) Trevor, D. J.; Chidsey, C. E. D. *J. Vac. Sci. Technol., B* **1991**, *9*, 964.

(23) Michely, T.; Besocke, K. H.; Comsa, G. *Surf. Sci. Lett.* **1990**, *230*, L135.

(24) Jaklevic, R. C.; Elie, L. *Phys. Rev. Lett.* **1988**, *60*, 120.

(25) Sette, F.; Hashizume, T.; Comin, F.; MacDowell, A. A.; Citrin, P. H. *Phys. Rev. Lett.* **1988**, *61*, 1384.

(26) Trevor, D. J.; Chidsey, C. E. D.; Loiacono, D. N. *Phys. Rev. Lett.* **1989**, *62*, 929.

# Scanning Tunneling Microscopy Studies of Au(111) Derivatized with Organothiols

### Yeon-Taik Kim, Robin L. McCarley, and Allen J. Bard*

*Department of Chemistry and Biochemistry, The University of Texas at Austin, Austin, Texas 78712*
*(Received: February 20, 1992; In Final Form: April 28, 1992)*

Atomic resolution scanning tunneling microscopy (STM) images of various-sized organothiols adsorbed on Au(111) display a $(\sqrt{3} \times \sqrt{3})R30°$ structure, even when the $\omega$-substituent size (4.3–13 Å) is so large that such a packing should not be possible. The observation of a $(\sqrt{3} \times \sqrt{3})R30°$ structure for thiols that should pack less densely suggests that the observed images are of gold electronic distributions that have been perturbed by the adsorbed thiol.

## Introduction

We report here atomic resolution scanning tunneling microscopy images of the Au(111) surface derivatized with various-sized organothiols (4-aminothiophenol, [Ru(bipyridine)$_2$(4-methyl-4'-(12-mercaptododecyl)-2,2'-bipyridine)](PF$_6$)$_2$, (C$_5$H$_5$)Fe(C$_5$H$_4$CO$_2$(CH$_2$)$_{16}$SH), [2]staffane-3,3'-dithiol pentaamine-ruthenium(II) hexafluorophosphate, and [2]staffane-3,3'-dithiol silver Figure 1) via self-assembly. The surface showed $(\sqrt{3} \times \sqrt{3})R30°$ superlattice structures regardless of the physical size of the substituent group of the thiol. The physical size of the $\omega$-substituent varied from 4.3 to 13 Å. The unexpected $(\sqrt{3} \times \sqrt{3})R30°$ structure, especially in cases where such a packing was prevented by the size of the $\omega$-substituent, is interpreted as electronic in nature and is caused by a spatial extension of Au wave functions on neighboring sites induced by the adsorbed species on the Au surface.

Following the invention of the scanning tunneling microscope (STM),[1] remarkable atomic and molecular structures have been elucidated in different environments such as air, liquid, and ultrahigh vacuum.[2] Recently, STM has been used to study the topography of organic monolayers formed by the Langmuir–Blodgett technique or self-assembly.[3] Because the STM is blind to the actual chemical nature of the adsorbed species and only responds to electron density, the images obtained can be easily misinterpreted while attempting to understand real topographic features. For example, images of the basal plane of highly oriented pyrolytic graphite (HOPG) obtained with the STM only show every other carbon atom because of an asymmetric electron density between adjacent carbon atom sites.[4] This difference in sites is intrinsic to graphite (0001) which has an AB stacking sequence. Moreover, another STM study of graphite showed long range electronic perturbations caused by defects or adsorbates.[5] The defects or adsorbates perturb the charge density resulting in an anomalous $(\sqrt{3} \times \sqrt{3})R30°$ superlattice structure. Such superlattice structures on HOPG were interpreted as a change in the electronic structure of carbon atoms rather than a lattice reconstruction. Furthermore, STM studies have yielded images

of graphite with a large scale hexagonal pattern with spacings varying from 4 to 110 Å, depending on the experimental conditions.[6] Charge density waves observed by STM with low dimensional materials are another example of electronic structures caused by a slight displacement of the atoms.[7] In this paper we suggest that the $(\sqrt{3} \times \sqrt{3})R30°$ structure on Au(111)/mica derivatized with a monolayer of organothiols is the result of Au electronic perturbations, rather than actual imaging of the monolayer itself.

## Experimental Section

**Chemicals.** The 4-aminothiophenol (4-ATP) was purchased from Aldrich and vacuum-sublimed prior to use. Staffane compounds ([2]staffane-3,3'-dithiol ([2]S-dithiol), [2]staffane-3,3'-dithiol pentaamineruthenium(II) hexafluorophosphate (Ru-[2]-S-dithiol)) were obtained from Professor Josef Michl, and detailed synthetic methods for these compounds are described elsewhere.[8] The [Ru(bpy)$_2$(4-methyl-4'-(12-mercaptododecyl)-2,2'-bipyridine)](PF$_6$)$_2$, abbreviated as Rub$_2$b*, and (C$_5$H$_5$)Fe(C$_5$H$_4$CO$_2$(CH$_2$)$_{16}$SH) were provided by Drs. Y. S. Obeng and D. Collard, respectively. Synthetic methods for these thiols can be found in the literature.[9,10] AgNO$_3$ (99.9999%) was obtained from Aldrich and used to make the staffane dithiol–Ag complex. Absolute ethanol and HPLC grade acetone were used without further purification. All other chemicals were reagent grade or better.

**Substrate Preparation and Monolayer Formation.** Approximately 150 nm thick Au(111) films were evaporated onto mica substrates as previously described.[11] Briefly, Au(111) films were prepared by thermal evaporation of high-purity Au (99.99%) at 0.2 nm s$^{-1}$ onto heated mica in a Plasmatron P-30 thin film system operating at $2 \times 10^{-6}$ Torr vacuum. The mica (Asheville-Schoonmaker, Newport News, VA) was heated to 310 °C and held there for 30 min before deposition was carried out. Once the substrates had cooled to near 100 °C, the chamber was back-filled with nitrogen and the Au/mica films were placed in ethanol (0.25 mM ferrocene thiol, 10 mM 4-ATP, 0.1 mM [2]-S-dithiol, and 0.1 mM Ru-[2]S-dithiol) or acetone (0.25 mM